MODELING AND CONTROL OF ELECTROSTATICALLY ACTUATED RF-MEMS SWITCHES

By

Omar A. H. Awad

A Thesis Presented to the Faculty of the
American University of Sharjah
College of Engineering
in Partial Fulfillment
of the Requirements
for the Degree of

Master of Science in
Mechanical Engineering

Sharjah, United Arab Emirates

February 2014

Approval Signatures

We, the undersigned, approve the Master's Thesis of Omar A. H. Awad.
Thesis Title: Modeling, and Control of Electrostatically Actuated RF-MEMS Switch.

Signature	**Date of Signature** (dd/mm/yyyy)
_____	_____
Dr. Ameen El Sinawi Associate Professor, Department of Mechanical Engineering Thesis Advisor	
_____	_____
Dr. Maher Bakri-Kassem Assistant Professor, Department of Electrical Engineering Thesis Co-Advisor	
_____	_____
Dr. Taha Landolsi Associate Professor, Department of Computer Science & Engineering Thesis Co-Advisor	
_____	_____
Dr. Nasser Qaddoumi Professor, Department of Electrical Engineering Thesis Committee Member	
_____	_____
Dr. Basil Darras Assistant Professor, Department of Mechanical Engineering Thesis Committee Member	
_____	_____
Dr. Ali Jhemi Assistant Professor, Department of Mechanical Engineering Thesis Committee Member	
_____	_____
Dr. Essam Wahba Interim Head, Department of Mechanical Engineering	
_____	_____
Dr. Hany El-Kadi Associate Dean, College of Engineering	
_____	_____
Dr. Leland Blank Dean, College of Engineering	
_____	_____
Dr. Khaled Assaleh Director of Graduate Studies	

Acknowledgements

In the name of Allah, the most gracious and most merciful.

First, I am most grateful to Allah for granting me the power and will to carry on and complete this research.

Although this thesis holds my name, I wouldn't have completed it without the support and help of numerous people. First, I would like to thank my family for the support I was given during my study period, especially my father, who always believed in me and kept pushing me forward. In addition, I would like to express my gratitude and special thanks to my advisor Dr. Ameen El Sinawi for his guidance, help, and supervision on this thesis. His insights on engineering systems always inspire those around him, and his encouragement and patience are what kept me working with him with great enthusiasm.

Secondly, I would also like to thank my co-advisers Dr. Taha Landolsi, from the Computer Engineering Department, who was a valuable asset both to me and to the research, and Dr. Maher Bakri-Kassem, from the Electrical Engineering Department, for his efforts and assist throughout this work.

To my lovely family & my true friends

for their endless love and support

Abstract

This work presents a novel approach to modeling and control of an RF-MEMS switch. The model presented in this work is comprehensive and generic in nature such that it takes into account the effect of squeeze film damping, impact force and electrostatic force effects on the dynamic behavior of the switch during pull-in and release of its membrane. This model makes it adaptable to any similar switch regardless of the form and/or dimensions. Simulation results of the switch dynamics is validated against experimental data for an identical switch. Model response to electrostatic voltage shows very good agreement with experiments. The proposed model is then used to construct a feedback controller capable of improving response parameters of the membrane during operation. Due to micro-dimensions of the switch, real time displacement measurement of the membrane is not readily available. Therefore, the proposed controller utilizes measurement of switch capacitors current as a platform for real time estimates of the membrane position. Membrane Current measurement was not available for control purposes due to the lack of the fabricated RF MEMS switch. Consequently, approximate model for current-displacement relationship is constructed from numerical solution of the nonlinear model data and system identification techniques using Simulink.

Table of Contents

List of Figures

List of Tables

Abbreviations

RF:	Radio Frequency
MEMS:	Micro Electro Mechanical System
PIN:	Positive-Intrinsic-Negative
SFD:	Squeeze Film Damping
SPST:	Single Point Single Throw
ARX:	Autoregressive eXogenous
ARMAX:	Autoregressive Moving Average eXogenous
SS:	State Space
ISS:	Input to State Stabilization
2DoF:	Two Degree of Freedom
PID:	Proportional-Integral-Derivative
R. H. S:	Right Hand Side
L. H. S:	Left Hand Side

Chapter 1 : Introduction

1.1 Problem Statement and Motivation

Despite the scientific breakthroughs in almost all aspects of technology, there are always minor issues that cause irritation. Modeling and control of RF-MEMS switches have always been a challenge, and yet a great importance. Although accurate models of different RF-MEMS switches have been achieved in some studies, with the use of some under estimating but convenient assumptions, not a great deal of work has been done that aims to control the switch actively. This is due to the fact that measuring the displacement of the switches' membrane is not readily available because of the size limitations. Controlling the switch is as important as it is modeling. However, being able to control such a device will unleash its true potential, making it the number one choice in electronic circuitry switches. RF-MEMS switches consume significantly less power than its counterparts, and if controlled, will have much better performance in terms of switching speed and life time. RF-MEMS switches tend to bounce off the substrate upon actuation, as well as vibrate heavily when released.

1.2 Objective and Scope of Work

The goal of this study is to develop a comprehensive and fully functional model, that takes into account all aspects of the switch's physical parameters, and provide alternative method to track the membrane's displacement using capacitor current. Extracting the values of the displacement from the current will aid in the design and implementation of an active controller that reduce response dynamics characteristics and reduce impact forces the switch experience upon actuation.

The Model's accuracy of Microelectromehcanical Systems (MEMS) at the design stage, is crucial to its functionality and durability during operation. Extensive research is being carried out to construct reliable and accurate models of Radio Frequency (RF) MEMS switches, due to the models importance in determining the switching time, transient characteristics [1], as well as energy dissipation mechanisms in these switches [2]. Significant research effort has focused on the effect of squeeze film damping (SFD) on the switch dynamic behavior, and the mechanism by which the squeeze film (SF) dissipates energy. The latter has proven to be difficult to model,

due to the vast variety of switch geometries and designs. However, it is common knowledge now that the SF adds stiffness and damping to the structure and, thus, has significant effect on the dynamic response of the switch membrane [2-6], therefore, it is important to determine switch resonance frequencies in the presence of SF within the switch gap. This also leads to a critical dilemma encountered during modeling which is whether to include the SF as part of the structure or add its effect after the SF-free structure is modeled. Both approaches have been used in the literature [1-2], however, neither approach has been followed as a standard. In the first part of this research work, we examine the following:

1. Effect of SF on resonance frequencies of the structure.
2. Effect of the impact force on the transient response of the switch membrane.
3. Effect of switch membrane perforation on switch overall damping.

Numerical Simulation of the proposed model is used to validate its integrity. Full comparison between model response to electrostatic voltage at pull in and release against experimental results is presented. Upon model verification, data relating capacitor current to membrane displacement obtained from the non-linear relation depicted by Eq. 1.1 is utilized to construct a control adaptable model:

$$i = \frac{\varepsilon_0 A V_{dc}}{(d-x)^2} \cdot \frac{dx}{dt} \tag{1.1}$$

The accuracy of the system obtained from system identification was found to be very high, around 95%.

Finally, the values of the displacement are used in a negative feedback loop, where a well-tuned two degree of freedom Proportional-Integral-Derivative (2 DoF PID) controller is constructed. The control task is to utilize displacement estimates obtained from the current measurements, to modify or control the membrane displacement by controlling the input voltage to the system, in order to slow the capacitor's plate velocity and avoid impact upon actuation; as well as eliminating the vibrations experienced by the switch once it is released i.e. the circuit is opened.

1.3 Thesis Outline

The framework of the current thesis is as follows: Chapter 1 includes an introduction of the thesis along with the problem statement, motivation, objectives, methodology and scope of work. In Chapter 2, historical background and literature review of MEMS and associated control theories are examined. Chapter 3 presents the first modeling approach along with the results obtained. Chapter 4 presents the final model and a step-by-step elaboration on the modeling and control, including effects of squeeze film damping, impact, and response characteristics. The aforementioned chapter also presents the system identification procedure needed to construct the model relation current to displacement in state-space form. Design construction of the control scheme is also presented and discussed in the latter chapter. Chapter 5 presents the results of different control approaches of the final model. Finally, Chapter 6 concludes the work done in this research and presents some of the future work.

Chapter 2 : Background

2.1 Historical Background

Over the last decade, the use of micro scale devices has increased. Such applications include, but not limited to, pressure transducers, actuators, high-speed switches, and tunable antennas [7]. While micro electro-mechanical devices are being integrated more often into electronic circuitry, RF MEMS switches show significant advantages over its solid state counterparts such as Positive Intrinsic Negative "PiN" switches, which are widely used in RF and Microwave switches. Not only do MEMS switches have better response characteristics, in terms of intermodulation distortion and lower RF losses; but they also consume significantly less power than PIN switches [7]. Moreover, vibrations due to actuation of the switch have significant effects on both its life and efficiency. It is also well established that vibration control of MEMS devices is not an easy task due to rapidly changing dynamics, nonlinearities, and difficulties associated with placing sensory devices on the MEMS switch [8].

In order to integrate MEMS switches in future applications, a sufficient understanding of the mechanical behavior of the MEMS switches has to be acquired, and a valid active control theory has to be presented that will help minimize the switches' vibrations, increase their efficiency and life. For a MEMS switch, the medium in which the switch is operating, strongly affects its performance, and plays a major role in its design and control. Some MEMS switches are designed to have large damping to avoid resonance response, which is likely to cause electrical or mechanical failures [9]. Energy dissipation in MEMS switches is evaluated from different perspectives, such as losses to the environment due to viscous damping, or acoustic radiation [9]. Thin air film interaction with structure, also known as the squeeze film, depends mainly on the structure's natural frequencies and mode shapes. The speed of the vibrating switch effects diffusion time of the gas filling the gap between the switch and the substrate. For example, if the membrane closes relatively slowly, the gas trapped between the switch and the substrate has enough time to escape, in this case the gas acts as a damper. On the other hand, if the membrane closure time is relatively fast, the air film has less time to defuse thus, it acts like a stiff spring.

There are various types of MEMS switches with various configurations depending on method of actuation, manufacturer, and switch application [10]-[13]. Geometry and analysis of the RF-MEMS switch under consideration is identical to [1]. The reason for this adaptation is to verify and compare the proposed modeling approach presented in this work with the experimental results reported in [1]. Although the modeling approach is generic and can be adopted for any switch geometry, the model presented herewith is verified for the geometry in [1].

2.2 Literature Review

Extensive studies have been done on the modeling of RF-MEMS switches. Majority of them are tackling the dynamics of the MEMS switch under the effect of squeeze film damping, while few incorporate impact forces in the modeling approach. As far as control is concerned, some studies show attempts to control the MEMS switch passively using a feed forward loop, which has proven to be sometimes useful, but not reliable due to the non-linearities presented in the model. A control attempt based on a feed forward loop might create instabilities in the system, thus causing failure. Below, we summarize some of the main contributions reported on the modeling and control of MEMS devices:

2.2.1 Modeling of RF-MEMS Switches

Niessner et al. [1] combined Reynolds equations for laminar flow with certain geometrical features to calculate the squeeze film damping effect at atmospheric pressure, on the dynamic behavior of the switch. In their work, the authors omitted the lateral velocities in the Couette flow since he assumed the plate is moving only in the vertical direction. The Reynolds equation was simplified but not enough to account for losses due to the perforations or pressure drop outside the perimeter of the membrane. In order to capture the full effect of the squeeze film damping, a finite network of the coupled system was utilized to evaluate the non-linear Reynolds equations where applicable. Their results showed excellent agreement with the experimental data.

Suijlen et al. [2] introduced an analytical model for the squeeze film damping of MEMS structures in the regime of free molecular flow. Their work established a relationship between the speed of the resonating MEM device operating in a volume

of air on one hand, and the damping and stiffness coefficients of the air on the other. The air contents were approximated as pure nitrogen in order to reduce the modeling complexity of the problem. The faster the motion of the membrane the less time the nitrogen molecules have to diffuse, causing the thin air film to act like a stiff spring. If the MEM structure moved slowly in the gap, the molecules have enough time to diffuse and thus act as a damper. The diffusion time is calculated analytically using the model of random walk Brownian motion. Numerically it is calculated using the Monte Carlo simulation of the ballistic trajectories of the molecules following the Maxwell-Boltzmann statistics and full thermal accommodation in gas-surface collisions. Comparing modeling results to experimental values returned less than 10% error.

Herrera-May et al. [3] analyzed the mechanical behavior of a resonant microstructure for magnetic applications, taking into consideration the effect of squeeze film damping. The microstructure consists of thin poly silicon beam elements, each with a 1.5 micro meter thickness by 20 micro meter width. The analysis was done under various magnetic field orientations at atmospheric pressure for both, finite element (FE), and mathematical models. In both mathematical and finite element models, the squeeze film damping was taken into consideration. The response of the micro-structure showed acceptable agreement between both models, indicating the validity of the FE model.

In Bao & Yang [4], the authors presented a survey of the work done on the effect of squeeze film damping. He discussed the mathematical models governing the squeeze film damping in perforated and slotted plates, the squeeze film damping in rarefied air, and in micro torsion mirrors. Such models are the non-linear isothermal Reynolds equation with different forms for different conditions. This work reviews the recent research done in this field and provides comparison between simulation and experimental results.

Younis and Yagubizade [5] examine the non-linear impact of squeeze film damping on mechanical response of a clamped-clamped MEM beam to mechanical shock. In their work, they solve multiple nonlinear Reynolds equations simultaneously, coupled with the nonlinear Euler-Bernoulli beam equation in order to model the squeeze film damping. For the solid domain, a Galerkin-based reduced-order model is utilized. For the fluid domain, a finite difference method is utilized. The results show that for shock impact, squeeze film damping can be used to

minimize the displacement of the micro structure upon release if the medium of operation is air.

Pandey et al. [6] modeled the squeeze film damping in perforated structures using a modified Reynolds equation that includes rarefaction effect and compressibility. Using a simple mapping function, they were able to linearize the previously mentioned equation and transformed it into two dimensional diffusion equations. Analytical solution is obtained using Green's function. The results of the squeeze film damping forces were compared to the solution of 3D Navier-Stokes equations solved using ANSYS. He reported good agreement.

LaRose & Murphy [7] modeled the Impact dynamics of clamped-clamped RF MEMS switches. Their model included inertial effects, structural and air damping, and impact dynamics between the switch's micro beam and the substrate. The model shows complicated behavior, including impact, sensitivity to initial conditions and its implications on periodic switching. However, the model was validated against experimental and numerical data and reliable results were reported. They suggested certain improvements in the model to simulate cyclic impact and fatigue loading.

Nayfeh and Younis [9] presented a new approach to modeling of flexible structures under the effect of squeeze film damping, utilizing compressible Reynolds equation. They coupled it with the equation governing the plate deflection and tested a clamped-clamped MEMS switch to calculate quality factors. They utilized the first 5 modes of vibration of in the analysis. Their model takes into account the electrostatic force between capacitor plates, restoring force, and slip condition at a very low pressure. The reported results are in excellent agreement with the experimental data.

McCarthy et al. [10], did an experimental study on both uniform and non uniform RF switches and modeled the dynamic behavior of these switches including contact bounce, using time transient finite difference method. Moreover, the damping forces were taken into account using the Reynolds equation. The switch was modeled using Euler-Bernoulli beam theory. McCarthy reported excellent agreement between theory and experimental results with respect to the initial pull in time. Duration of the first bounce was also obtained. Uniform switch is simply a beam made of gold plated nickel that closes the circuit upon actuation. The non-uniform switch is made of pure gold.

Parallel plates micro accelerometer was designed and modeled by Seidel et al. [14] utilizing the harmonic oscillator concept along with constant damping

coefficient. They concluded that there was a mismatch between the theoretical frequency response curves and those obtained experimentally.

Newell [15] analyzed the effect of different film pressure value on the damping of cantilever resonators. The author divided the pressure range from vacuum to atmospheric pressure into three regimes. Low pressure (near vacuum), medium pressure, and high pressure (near atmospheric). Newell derived an expression for damping based on the pressure drop in a viscous fluid flowing through a parallel-walled duct.

Experiments were conducted by Zook et al. [16] on electrostatically actuated clamped-clamped MEMS switch captured at low pressure. They used Newell model [15] in their modeling approach. However, their results did not match the experimental data.

Zhang and Zhao [17], presented an improved model for the fixed-fixed RF MEMS switch, as shown in Figure 4, by taking into consideration axial stresses, residual stresses, and fringing field effect of the structure. They discussed the models available for the RF MEMS switch such as the 1D lumped model which considers the switch as a spring mass-damper as shown in Figure 5, and 2D distributed model which takes into account the fringing field, redial stresses, and axial stresses separately. Zhang's model, the 2D distributed model was utilized and refined in order to account for the previously mentioned parameters simultaneously. In addition, the resulting governing equation was dimensionless; to further facilitate analyzing the model. Zhang validated his propose model with experimental results of the fixed-fixed RF MEMS switch, showed the significance of axial and residual stresses and fringing field effect to the results of his model.

Niessner et al. [18] simulated the dynamic behavior of an RF-MEMS switch based on modal analysis obtained using ANSYS and MATLAB. In ANSYS, the mechanical Finite Element analysis of the model was generated, and a modal analysis was done. The results were later imported into MATLAB to carry on with the dynamic analysis of the MEMS switch. The authors took into consideration viscous damping forces and contact forces in their model. After comparing the results obtained with the experimental data, it was found that results agree in quasi-static pull in characteristics, and with non-contact transient measures at low ambient pressures. On the other hand, the model fails to mimic the behavior of the switch with the presence of contact due to lack of accuracy in impact force modeling.

2.2.2 Controlling MEMS Devices.

MEMS devices started in 1960s when the first open-loop pressure sensors were developed [19]. A great deal of inventions resulted from the successful integration of MEMS and integrated circuits such as gyro-sensors, accelerometers, devices for High Definition Television displays, inkjet print heads, and drug delivery systems [21]. New MEMS applications are emerging with successful integration of different fields of engineering. However, despite MEMS small dimensions, MEMS are not less complicated than skyscrapers and bridges.

According to Janusz Bryzek keynote talk, CDC 2003, Maui, Hawaii, he said "Most MEMS technologists do not have a background in control technology. Without the help of control systems engineers, development cycles will be stretched" [20].

Proportional-Integral-Derivative (PID) controllers are the most dominant and effective form of automatic-controllers in to industrial applications. Using this type of controllers requires specific tuning for the proportional, derivative, and integral gains. For example, different systems require different gains to yield optimum response. This process is called controller tuning. This is relatively easy to achieve using tuning rules [21]. Feedback control showed an outstanding impact on the mechanical performance of various systems, and will continue to do so in the future. With the emerging technologies of automatic tuning and the fact that PID controllers are widely used in the industry, using PID control to control the RF-MEMS switch [22, 23] .

Izadbakhsh et al. [24] present three new approaches controlling MEMS optical switch. These approaches are, Sliding Mode Control, High Gain Control, and Model Free- Based Control. The last two are considered novel in this field. In their work, they found that all three controllers are robust against some uncertainties such as external disturbance and modeling errors. The main advantages of the model free and high gain approaches are their simplicity in design, and the relatively-less computational burden associated with them. Zhu et al. [25] present similar work to that of Alireza [24] but with different controller approaches. They utilized the input to state stabilization (ISS) and robust back stepping techniques. This work shows satisfactory performance and robustness when parametric uncertainties are presented.

Seleim et al. [26] used a feed backward closed loop in order to control the chaotic region of a MEMS cantilever beam. The chaotic region is a region where the

actuation voltage is close to the pull-in voltage, yet not sufficient enough to close the circuit. Operating within the chaotic region will cause the system to become unstable and will allow for pull in when any external disturbance occurs. The authors found that, utilizing feed backward controllers is necessary to operate in the chaotic region, and that experimentally measured controller output is in good agreement with the simulation results.

Borovic et al. [27] attempted to control a MEM optical switch using PD controller and feed-forward, to obtain a fast optical switching with minimal overshoot. Their mathematical model consisted of a Mechanical Model, Electrical Model, and Optical Model. While the electrical and optical models are very accurate, the mechanical model was found to be inaccurate in terms of damping. This caused their model to deviate from the experimental, with results that are far from accurate. Even though their model is inaccurate, they proceeded with controller design and improved the response of their model. However, one should not over look the fact that adding a feed-forward is not a wise choice when it comes to applications with significant nonlinearities. The feed-forward technique might cause the system to become unstable.

This research presented here is the first to discuss active control of RF MEMS switch. Since sensing the motion of micro structures is difficult, there has been no research work on active controlling of the RF-MEMS switch. However, the approach stated here is very effective theoretically; experimental work is yet to be done.

Chapter 3 : SPST-RF Modeling

3.1 Finite Element Method

The design of MEMS systems controllers relies heavily on the availability of an accurate dynamical model. However, it is very difficult to obtain an accurate dynamical model of MEMS through fabrication and testing. Analytical models are almost always inadequate since incorporating all the dominant forces is a challenging task. That is when Finite Element Analysis (FEA) becomes the best modeling approach. Nevertheless, using a full FEA model that includes mechanical, electrical, and thermal modeling can be a difficult task, instead, a reduced order model is used. FEA simulation is carried out on ANSYS, utilizing the following to create a state-space model: The flexible structure is represented in nodal coordinates by the following second order matrix differential equation:

$$M\,\ddot{q} + D\,\dot{q} + K\,q = B\,w \tag{3.1}$$

$$Y_s = C_d\,q + C_v\,q \tag{3.2}$$

In the above equation q is the nx1 displacement vector, w is the mx1 external input vector, Y_s is the px1 nodal output vector, M, D, and K are the nxn mass, damping, and stiffness matrices, respectively. C_d and C_v are respectively, the pxn output displacement and output velocity matrices. The mass matrix is positive definite and the stiffness and damping matrices are positive semi definite. The damping matrix D is assumed to be proportional to the stiffness matrix K without any significant effect on the integrity of the model [8, 28]. Such dynamic model is usually obtained from finite-element codes and has the dimension n which is unacceptably high to use in producing a state-space model suitable for structural control. Therefore an alternative approach is to use an N-dimensional second-order modal model of the system where N << n. A second order modal-model of the system can be expressed as:

$$\ddot{\eta} + 2\,\Delta\,\Omega\,\dot{\eta} + \Omega^2\,\eta = B_m\,w \tag{3.3}$$

$$Y_s = C_{md}\,\eta + C_{mv}\,\dot{\eta} \tag{3.4}$$

Where $\eta = \Phi\, q$, and Φ is the nxN modal matrix, Ω is the NxN diagonal matrix of modal natural frequencies, Δ is the NxN modal damping matrix, B_m is the Nxm modal input matrix, C_{md} and C_{mv} are the pxN modal displacement and rate matrices, $z = [z_1\ z_2]^T = [\eta\ \dot{\eta}]^T$, flexible structures having point force(s) as the input(s) and point displacement(s) as output will have the state space representation, where $Y_s(t)$ and w(t) are the nodal output and input vectors respectively. Matrix D_u is the pxm feed through matrix. Equations 3.3 and 3.4 can also be represented by the following compact form,

$$\dot{z} = A(\theta) + B(\theta)w \tag{3.5}$$

$$Y_s = C(\theta)z + D_u(\theta)w \tag{3.6}$$

Where A, B, C, and Du matrices are functions of the system natural frequency, damping ratio, and mode shapes i.e $.\theta = f\ (\ \omega_i, \zeta_i, and\ f_i\ )_i = 1 \ldots N$. The dimension of this state-space representation is 2N and it is much more manageable than the 2n state-space model obtained from the corresponding nodal model. Detailed information on constructing state space model from natural frequencies and mode shapes is given in Younis et al. and Pandey et al. [5, 6].

The first model is adapted from McCarthy et al. [10]. The reason for choosing this model is that both, switch's dimensions and simulation results of its mechanical behavior are available. The switch is shown in Figures 3.1 and 3.2.

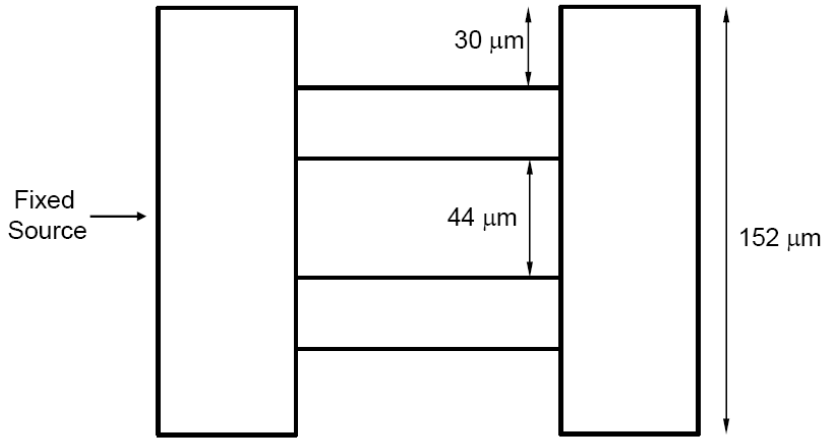

Figure 3.1 - Top view of the switch

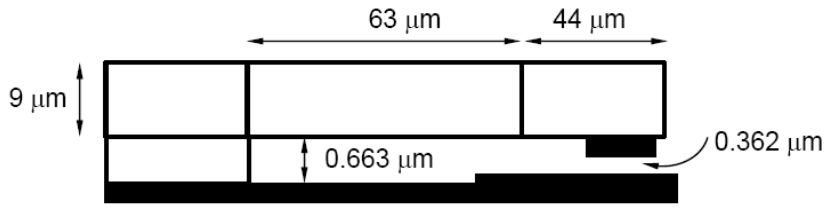

Figure 3.2 - Side view of the switch

A modal analysis is done for the first 15 modes in the frequency range of 1Hz to 100 MHz. Since the first modes require less energy to excite, they are most likely to have a larger norm and thus become dominant over other modes. A model reduction technique is implemented on the data. The modes that are retained are those with the largest norm, this technique is called the Hankel norm method [8]. The most dominant modes are the first, second, and fourth. Other modes returned a significantly lower norm values relative to the dominant ones, indicating that their contribution to switch dynamics is minimal and therefore, could be ignored. However, for the sake of accuracy, the first 5 most dominant modes where considered in the analysis, which are first, second, fourth, seventh, and twelfth.

Table 3.1 below lists the Hankel norm for each mode.

Table 3.1- Modal reduction

Mode	Frequency [Hz]	Hankel Norm
1	148000	0.0139
2	283000	0.0039
3	762000	0
4	898000	0.0001
5	1240000	0
6	1700000	0
7	2140000	0
8	2320000	0
9	2740000	0
10	3120000	0
11	3550000	0
12	3560000	0
13	3640000	0
14	4580000	0
15	5370000	0

The switch is modeled as operating at atm pressure. The resulting characteristic equation governing the behavior of the MEM switch is non-linear second order Ordinary Differential Equation with the following form,

$$M\,\ddot{x} + B\,\dot{x} + K\,x = F_e \tag{3.7}$$

Where M is the mass of the moving plate, B is the total damping coefficient consisting of both, materials damping and squeeze film damping. K is the total spring constant, and Fe is the electrostatic force.

3.2 Squeeze Film Damping Effect

The dynamic behavior and dynamic response of RF-MEMS switches are governed by both inertia of the system, squeeze film damping and spring characteristics. The gas molecules trapped between the capacitor plates heavily affect the response of this system. Squeeze film damping characteristics can be described by Reynolds equations. Depending on the complexity of the system, Reynolds equations can either be solved analytically giving exact results, or numerically using computational methods. The simpler the system, the easier it is to model the squeeze film damping effect [29].

The squeeze film damping model incorporated in this work and all associated equations are taken from Suijlen et al. [2] who state that the increase in gas density within the gap between the capacitors' plates is the driving force. Equations expressing the values of spring constant and damping co-efficient depend on the natural frequencies of the system and the random walk diffusion time of air molecules. As mentioned in section 2.1 the membrane velocity affects the behavior of air molecules within the switch gap, and thus governs the squeeze film effect on the dynamic behavior of the switch. Since air consists of 71% Nitrogen, it is assumed that the molecules within the switch gap are Nitrogen [N_2]. Equations used to calculate the effect of squeeze film on the model are expressed as follows:

$$B_{sq} = \frac{p\,A\,\tau}{d\,(\,1 + (\,\omega\tau\,)^2)} \tag{3.8}$$

$$K_{sq} = \frac{p\,A\,(\omega\tau)^2}{d\,(\,1 + (\,\omega\tau\,)^2)} \tag{3.9}$$

Where p is the atmospheric pressure, d is the gap between the actuator and plate, A is the membrane area, τ is the diffusion time for Nitrogen, and ω is the frequency of vibration.

τ is calculated using the following equation:

$$\tau = \frac{8\,A}{\pi^3\,d\,\upsilon} \tag{3.10}$$

Where υ is the average velocity of nitrogen molecules, and is calculated as follows:

$$\upsilon = \left(\frac{8\,K_b\,T}{\pi\,m}\right)^2 \tag{3.11}$$

K_b is Boltzmann's constant, T is the temperature in Kelvin [K], and m is the molecular mass of Nitrogen. Applying these equations to our model, the resulting diffusion time is 13.85 micro-seconds.

Values of K_{sq} and B_{sq} are calculated for the most significant modes of vibration. The results are listed in Table 3.2. It is clear that values of B_{sq} are negligible when compared to the corresponding values of K_{sq}.

Table 3.2 - Squeeze film constant values

Mode	K_{sq}[N/m]	B_{sq}[N.s/m]
1	1772.6	0.000148
2	1780.4	0.0000405
4	1783	0.000004
7	1783.3	0.0000007
12	1783.3	0.0000003

Finally, values obtained for both K_{sq} and B_{sq} are added algebraically to the system's natural stiffness and damping.

3.3 Electrostatic Force

The electrostatic force is the force exerted between the two capacitor plates that draw the membrane downwards to close the circuit; and is presented as follows:

$$F_e = \frac{\varepsilon_0\,A\,V^2}{\left(d_e - x(t)\right)^2} \tag{3.12}$$

Where ε_0 is the permittivity of air, A is the overlapping area of the membrane and the electrodes, V is the electrostatic voltage, d_e is the initial gap between the capacitor plates, and $x(t)$ is the displacement of any point on the membrane in the direction perpendicular to the electrodes. In this model the distributed electrostatic force is lumped and is applied on two nodes during the simulation, each experiences half of the total force.

3.4 Comprehensive Model

The final model includes the dynamics of the structure and squeeze film lumped together as follows:

$$B_{model} = B_{material} + B_{sf} \tag{3.13}$$

$$K_{model} = K_{material} + K_{sf} \tag{3.14}$$

The material is assumed to have 5% damping co-efficient (ξ =0.05), and its stiffness and damping are calculated as follows:

$$B_{material} = 2\,\zeta\,\omega_n\,M \tag{3.15}$$

$$K_{material} = \omega_n^2\,M \tag{3.16}$$

Where ω_n is the natural frequency of the system, and M is the mass of membrane. Squeeze film damping and co-efficient considered are for the dominant modes of vibration mentioned in section 3.1.

After finding K_{model} and B_{model}, Eqs. 3.15 and 3.16 are applied to find the corresponding ω_n and ζ for the comprehensive model. These values are used to construct the state-space model. The latter approach merges between the dynamics of squeeze film and structure into one model, stating how the response of the switch would be when actuated in air under atmospheric pressure. This only holds true as long as the membrane is moving towards the substrate and before impact occurs.

3.5 Simulation Results

The software used for simulating the dynamic behavior of the proposed model is MATLAB. A schematic of the block diagram used in the simulation is shown in Figure 3.3. The electrostatic force is applied to the state-space model, which includes the dynamics of the squeeze film as well.

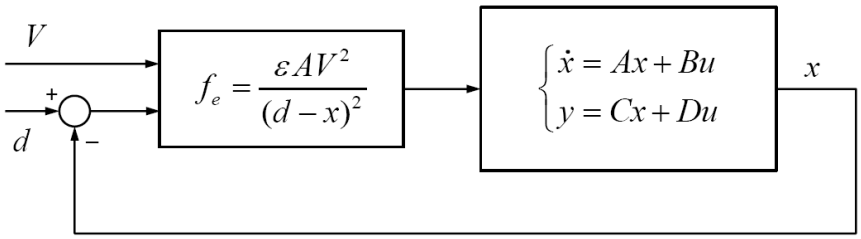

Figure 3.3 - Full set up used in experimental work

The following sections present the simulation results obtained from the SPST RFMEMS model.

3.5.1 Modal Reduction Verification

At the beginning of the analysis, it is crucial to make sure that the five vibration modes utilized are sufficient to capture the behavior of the switch. This is verified through comparison between the dynamic responses of a model with 15 modes and another with 5 modes with and without the effect of the squeeze film damping, for various voltages. As shown in Figures 3.4 and 3.5 shown, using reduced order model is sufficient to capture the behavior of the switch when compared to the full 15 modes model.

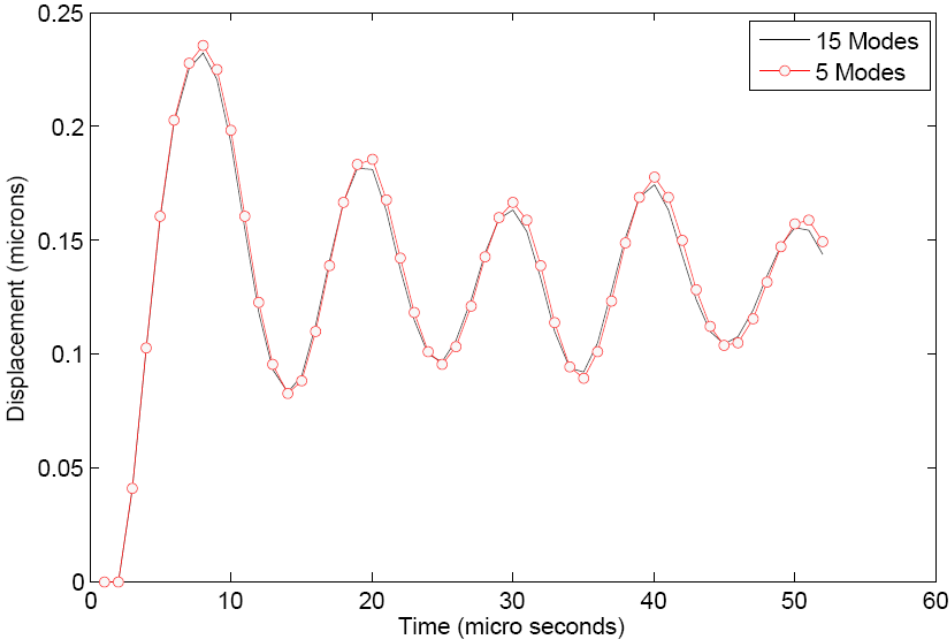

Figure 3.4 - Membrane displacement 22V without squeeze film damping

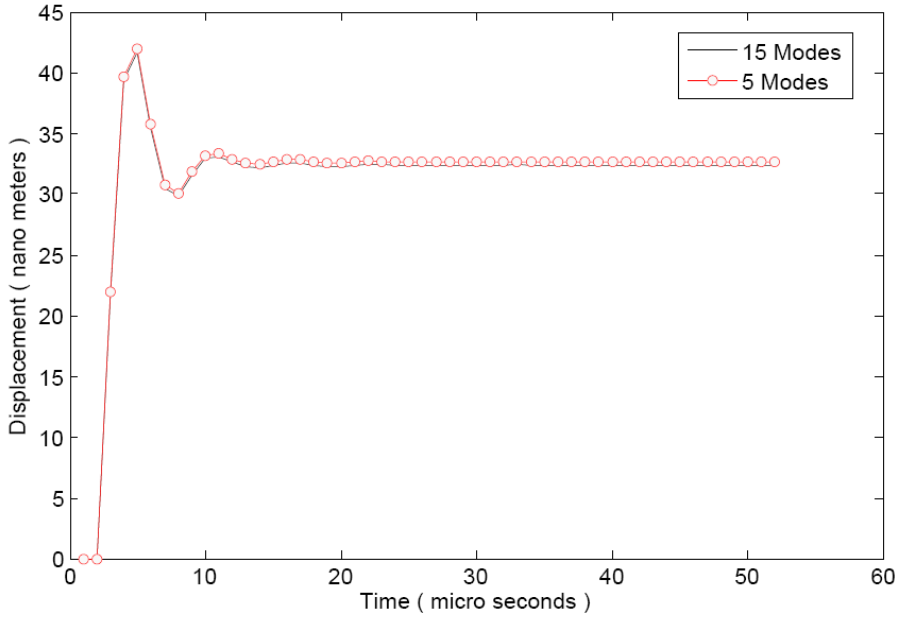

Figure 3.5 - Membrane displacement 22V with squeeze film damping

3.5.2 Squeeze Film Model Testing

The effect of introducing the squeeze film damping to the non-uniform switch governs the mechanical behavior of the switch, increasing the stiffness of the switch and damping, allowing it to settle quickly. Simulation shows that the SF-free switch model has a pull in voltage of 23 V. However, when incorporating the effect of the squeeze film into the model, the switch becomes stiffer and its damping increases. Therefore, the switch remains open, which holds true only in the transient state of the simulation, and once steady state is reached, the effect squeeze film should disappear. This result raised some doubts on the reliability of the squeeze film damping model used, and whether it is a valid assumption to lump the squeeze film model along with the dynamical model, as it is done in this case. These results are shown in Figures 3.6 and 3.7.

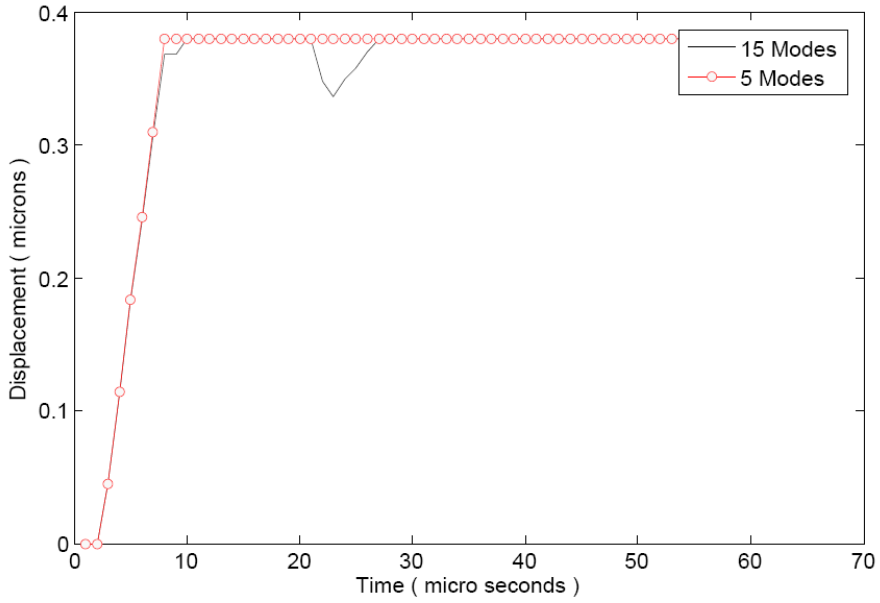

Figure 3.6 - Membrane displacement 23V without squeeze film damping

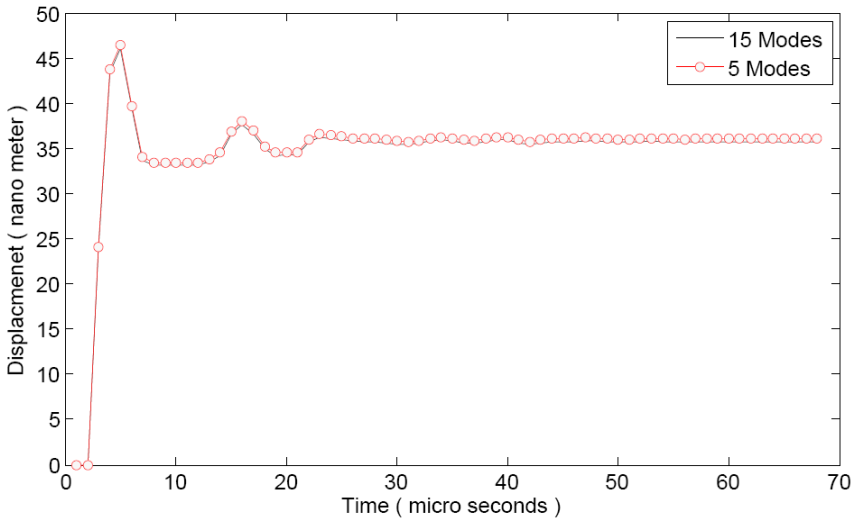

Figure 3.7 - Membrane displacement 23V with squeeze film damping

3.5.3 Comprehensive Model Testing

The introduction of squeeze film adds damping to the overall model, minimizing significantly the over shoot, as explained in the following equation:

$$OS = exp\left(\frac{-\zeta\pi}{\sqrt{1-\zeta^2}}\right) \times 100\% \tag{3.17}$$

Where OS is the overshoot percentage. It is clear how the relation between overshoot and damping is inversely proportional. In addition, since the switch is moving very fast, it does not allow the switch to close the circuit before bouncing several times. This approach gives a more accurate model when compared to real experimental values. Simulation shows that pull-in voltage is found to be 38 V as shown in Figures 3.8 and 3.9, which is very close to the value 36 V reported in [10]. Although some errors are present in the model, it returned quite accurate and reliable response which could be improved to mimic the exact behavior of the non-uniform switch in real life. These errors are due to some approximations and assumption in the model such as the approximation of the model in the 15 modes, the assumption of the medium being nitrogen instead of air, and the assumption of 5% natural damping in the material.

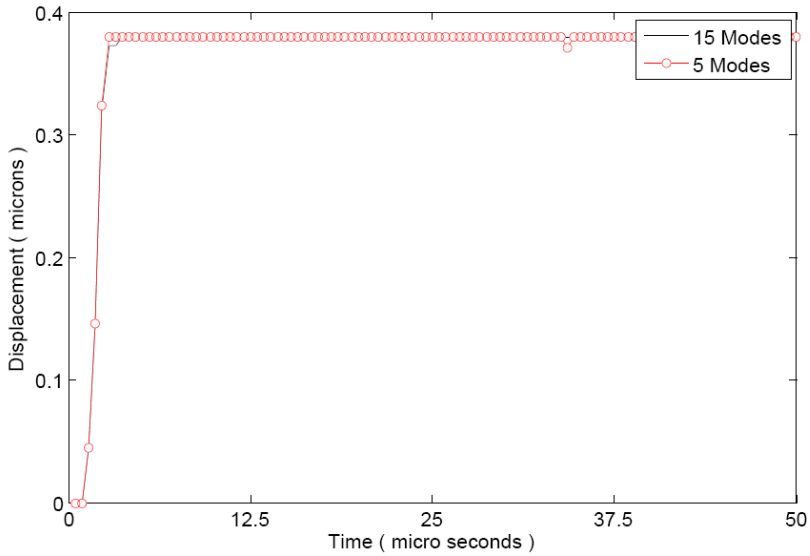

Figure 3.8 - Membrane displacement 38V without squeeze film damping

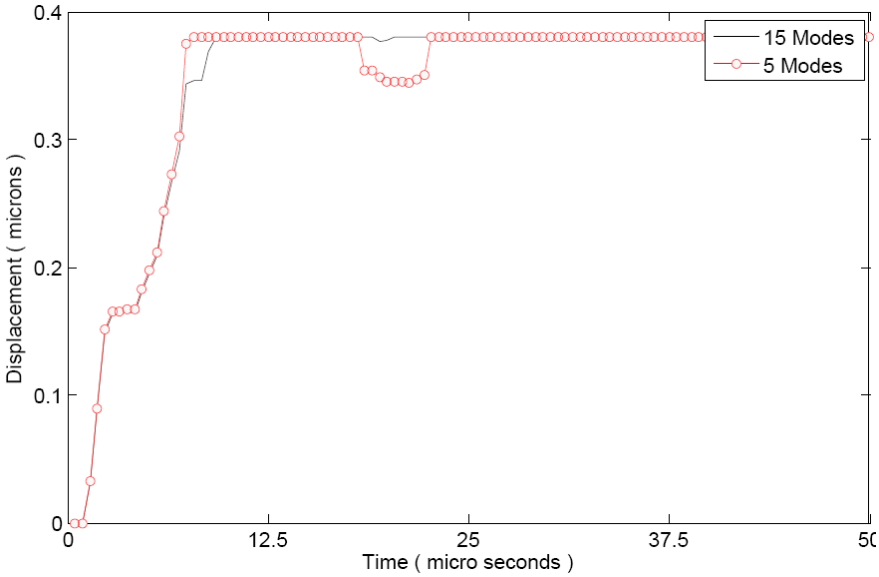

Figure 3.9 - Membrane displacement 38V with squeeze film damping

Chapter 4 : Perforated Membrane RF-MEMS Model

4.1 Finite Element Method

As mentioned in section 3.5, the switch shown in Figures 4.1 & 4.2 is adopted from [1], with dimensions listed in Table 4.1 for convenience.

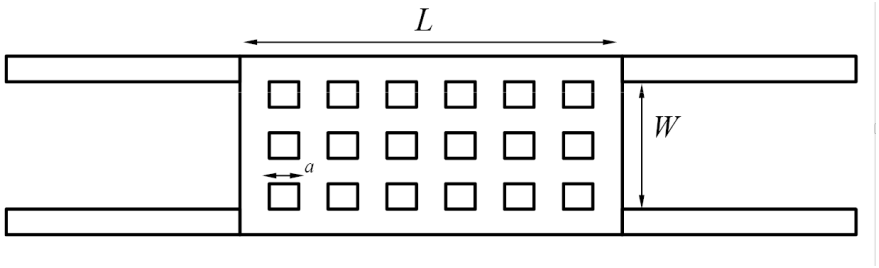

Figure 4.1 -Top view of the switch

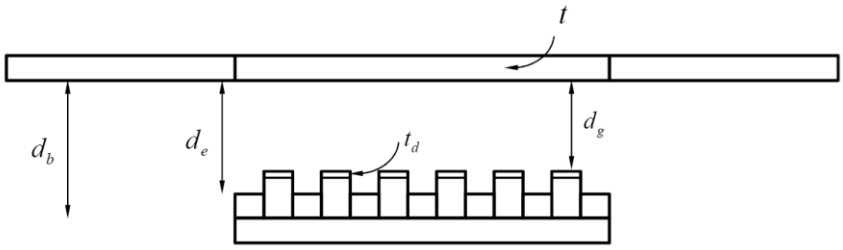

Figure 4.2 - Side view of the switch

Table 4.1 - Geometrical values of the switch under study in micrometers

Length(L) × Width (w) × Thickness (t)	250 ×140 ×5.2
Side length of the square holes (a)	20
Spacing between holes	20
Suspension beams Length(L) × Width (w) × Thickness (t)	165 ×10 ×2
Membrane to contact pads $\mathbf{d_g}$	1.7
Membrane to electrode $\mathbf{d_e}$	2.7
Membrane to base $\mathbf{d_b}$	3.4
Residual air gap $\mathbf{d_r}$	0.02-0.05

The model is constructed using FEA as presented in section 3.1. Modal analysis is done on the structure to determine the first ten modes of vibration. Nodal displacements data are utilized to construct the state space model of the system. Afterwards, a modal reduction is carried out to determine the dominant modes, which turned out to be the first, third, and fifth modes. Below is a table listing the Hankel norm for each mode.

Table 4.2 - Modal reduction

Mode	Frequency $[Hz]$	Hankel Norm
1	148000	0.3514
2	30293	0.0003
3	40965	0.0725
4	81358	0
5	135000	0.0031
6	139000	0
7	214000	0
8	231000	0.0005
9	263000	0.0001
10	276000	0.0008

The reduced order model decreases the computational speed without compromising the accuracy of the model.

Modal frequencies and mode shapes FEA are those of the system without incorporating the squeeze film effect, or the impact force (i.e. membrane operating in vacuum with no drain). The effect of squeeze film and impact forces are incorporated in the model later on.

In this model, the switch is to be operating at atm pressure [1]. Dynamic equation governing the behavior of the MEMS switch is non-linear second order ODE of the form,

$$M\,\ddot{x} + B\,\dot{x} + K\,x = \sum\left(F_e + F_{sfd} + F_{impact}\right) \tag{4.1}$$

Where M is the mass matrix of the moving plate, B is the total damping coefficient matrix consisting of both the materials damping and the squeeze film damping. K is the total stiffness matrix. Right Hand Side of Equation 4.1 represents all forces acting on the membrane. These will be explained in the following sections of this chapter.

4.2 Electrostatic Force

Membrane actuating electrostatic force is expressed in [30] as:

$$F_e(t) = \sum_{1}^{R} \left(\frac{\varepsilon_0 \, A \, V^2}{2 \left[\left(\frac{td}{\varepsilon_r} \right) + d_e - x(t) \right]^2} \right) \tag{4.2}$$

Where ε_0 is the permittivity of air, A is the overlapping area of the membrane with the electrodes, V is the switch electrostatic voltage, and x(t) is the displacement of any point on the membrane in the direction perpendicular to electrodes. ε_r is the permittivity of the dielectric material on the electrodes, and td is the thickness of this dielectric material. The summation in Equation 4.2 is over R electrodes.

4.3 Squeeze Film Damping Effect

The squeeze film spring and damping coefficients are found using the method presented by [31]. For a perforated membrane, equations read as :

$$\gamma_{sf} = \frac{3 \, \eta_{eff} \, a_c^2 \, A}{2 \, d_e^3} \, H(\gamma) \tag{4.3}$$

Where γ_{sf} is squeeze film damping coefficient. The variables in Equation 4.3 are defined with reference to Figure 4.3.

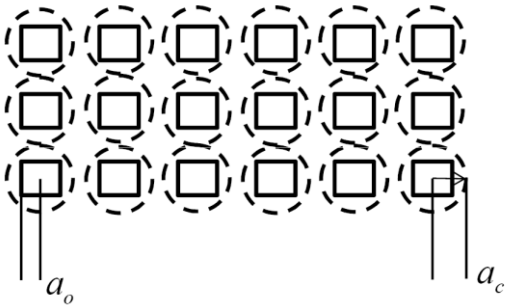

Figure 4.3 - Perforated membrane

Where a_c is the radius of the cell occupied by the hole, ao is the equivalent radius of the square hole, and $H(\gamma) = 4\,\gamma^3 - \gamma^2 - 4ln\gamma$ with $\gamma = \frac{a_o}{a_c}$

$$K_{sf} = \frac{64\,\sigma\,p\,A}{\pi^8\,d_e} \sum_{m,nodd} \frac{m^2 + c^2\,n^2}{(mn)^2\left[(m^2 + c^2\,n^2) + \frac{\sigma^2}{\pi^4}\right]} \tag{4.4}$$

Where K_{sf} is the squeeze film stiffness coefficient, p is the pressure, c is the membrane width to length ratio W/L, m and n are odd numbers, and σ is the squeeze number defined as;

$$\sigma = \frac{12\,\eta_{eff}\,W^2}{p\,d_e^2}\,\omega \tag{4.5}$$

Where ω is the frequency of vibration. In Equations 4.5 and 4.3, the effective viscosity of the squeeze film is denoted by η_{eff} which is also given by [8, 31, 37, 38] as:

$$\eta_{eff} = \frac{\eta}{1 + 9.638K_n^{1.159}} \tag{4.6}$$

Where $K_n = \gamma_p\ /\ d_e$ is the Knudsen number and γ_p is the mean free path of SF molecules. Equation 4.6 is valid for (K_n << 0:1), and η is the viscosity of the SF medium under normal conditions.

4.4 Impact Forces

Impact force in this switch results when the membrane contacts the contact pads as shown in Figure 4.4.

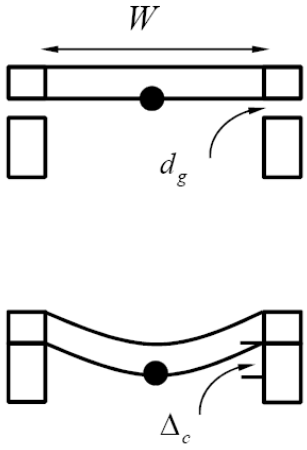

Figure 4.4 - Deflection of membrane upon contact

Upon contact, certain points on the edges of the membrane hit the contact pads and eventually come to a halt. However, nodes in the middle of the plate and specifically the point in the center of the membrane, under the effect of the membrane inertia, continue to move towards the electrode until a force balance on this point is reached. The force balance is achieved when the electrostatic force acting at the midpoint is nullified by an equal and opposite force. Examining the shape of the membrane, and considering the fact that among all the effective modes found for this switch, the first mode is the only one that is purely symmetric in the direction of the membrane motion. Therefore, the forces due to impact, and in reference to Figure 4.4, can be modeled as an elastic force due to the bending of the membrane in direction of minimum radius of gyration, and a damping force due to the squeeze film acting at the bottom of the membrane in the direction opposite to that of the membrane motion as in Figures 4.5.

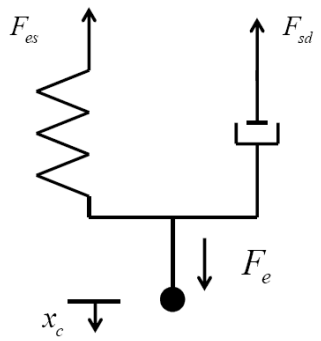

Figure 4.5 - Impact mechanics

The two forces shown in Figure 4.5 are modeled as:

$$F_{es} = K_{es}\Delta_c \tag{4.7}$$

$$F_{sd} = \frac{\gamma_{sf}}{R}\frac{d\,\Delta_c}{dt} \tag{4.8}$$

Where Δ_c is the displacement of the center point beyond the contact pads, while K_{es} is defined as the elastic stiffness of the membrane in the direction of minimum radius of gyration , and expressed in [32] as:

$$K_{es} = \frac{48\ E\ I_{min}}{W^3} \tag{4.9}$$

Where E is the modulus of elasticity of the membrane material, $I_{min} = (L - N\,.\,a\,)t^3/12$ is moment of inertia for the membrane cross-section, and N is the number of holes in the membrane. Equations 4.7 and 4.8 have values if and only if $\Delta_c = (x_c - d_e\,) > 0$ (i.e. when impact occurs). x_c is the membranes center-point displacement.

4.5 Effects of Squeeze Film Stiffness Coefficient on Membrane Resonance Frequencies.

It is clear that K_{sf} is dependent on the frequency of vibration, and in some special cases [31], it is directly proportional to ω^2. Therefore, the presence of the squeeze film will add stiffness to the structure, giving a rise to modal frequencies of the SF-free structure. The contribution of K_{sf} to modal frequencies of the structure can be modeled as:

$$f_{im} = f_i + \frac{1}{2\pi}\sqrt{\frac{K_{sf}}{m_{im}}} \tag{4.10}$$

Where f_{im} is the modified modal frequency for mode (i), f_i is the modal frequency obtained from ANSYS for the SF-free structure, and m_{im} is the effective modal mass for i^{th} mode [33].

4.6 System Identification

In control engineering, system identification is a diverse field that uses statistical analysis to build various mathematical models for dynamical systems. Generally, system identification uses curve fitting from measured input and output data for systems with unknown, or very difficult to obtain, mathematical models. Using the data at hand, different models are created with different accuracies. Obviously the higher the accuracy, the better the model is [34].

Since the displacement of the capacitor plate is very difficult to be tracked, a relation between the displacement and the current is derived, which would provide values of the displacement based on the input current. This is made because the current is relatively easy to measure in real life MEMS applications. The following is the derivation of the relation mentioned above:

$$V_{dc} = \frac{1}{C}\int i\, dt \tag{4.11}$$

$$C = \frac{\varepsilon A}{(d - x)} \tag{4.12}$$

Combining equations 4.11 and 4.12, and deriving both sides of the resultant equation we get:

$$i = \frac{\varepsilon A V_{dc}}{(d-x)^2} \frac{dx}{dt} \tag{4.13}$$

Where ε is the permittivity of air, A is the area of the capacitor plate, V_{dc} is the voltage applied across the capacitor plates, d is the initial gap, x is the displacement of the capacitor plate, and dx / dt is the velocity at which the capacitor plate is moving at.

Firstly, the system is excited at 20 V sine wave with a frequency of 200 Hz, which is below the pull in voltage, in order to capture the transient response with all the system dynamics. Afterwards, equation 4.13 was used to extract the behavior of the current in the circuit. Figure 4.6 shows the response of the system excited and the corresponding current values obtained from the variation of the position and the velocity. Now that the values of the current are in hand, which will be measured in real life applications, a state space model is needed to convert the current into displacement.

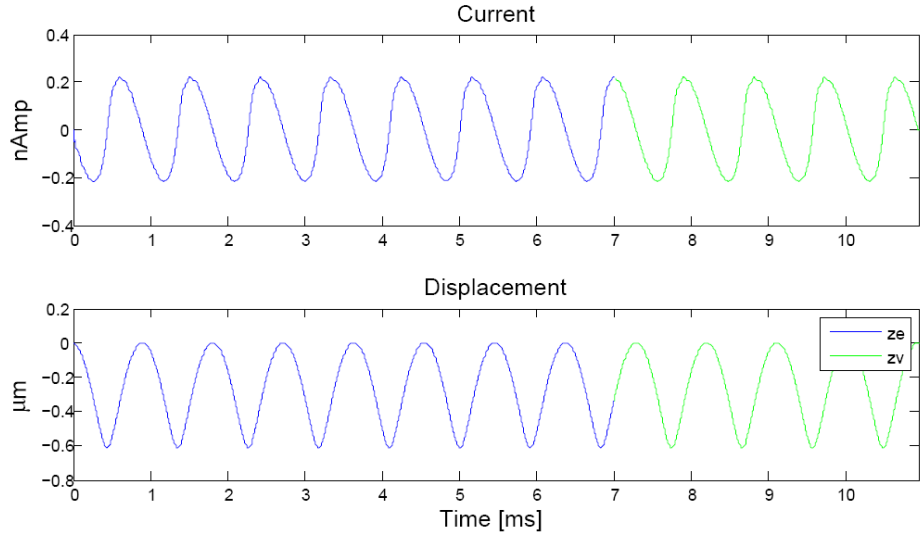

Figure 4.6 - Non-linear data obtained on displacement and current

The system identification tool in MATLAB is used to construct this model. Ze are the values used for estimation, and Zv are the values used for validation. The system identification tool generated a 98% accurate ARX model. The ARX model is

converted into a state space model using the ss(ARXMODEL,' MEASURE') command. This is the only available command, however, it compromises the accuracy of the model since it removes all the noises in the model after conversion. In addition, in such small scale complicated models, the noise might correspond to the mechanical behavior of the system, and thus it should not be removed. The state space model is then imported to MATLAB and tested for validity. The simulation is carried over at the pull in voltage of 35 V. Figure 4.7 represents the behavior of the model acquired from the system identification. As expected, even though the pattern is similar to the real model, the response is not accurate.

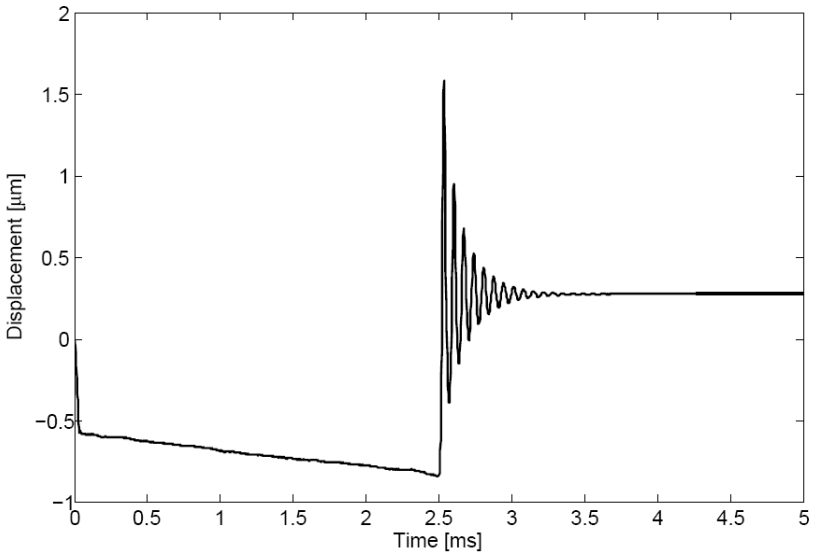

Figure 4.7 - Non-linear data obtained on displacement and current

4.6.1 Two Degree of Freedom PID Controller

The degree of freedom of a control system is defined as the number of closed-loop transfer functions that can be adjusted independently [35]. Control Systems design is considered as a multi-objective problem, this gives the two degree of freedom (2DoF) Proportional-Integral-Derivative (PID) controller advantage over the one degree of freedom PID controller. The two degree of freedom controller is a two input one output system, where the inputs are a set point (i.e. the required system behavior), and a variable (i.e. the system needs to be controlled) compared against each other. The controller parameters are tuned, different techniques are available from optimal tuning of 2DoF PID controllers, to enhance the variable system response and make it as similar as it could be to the set point system [36].

The two degree of freedom PID controller operates in the feed forward path and a feedback loop. The controller receives two signals, a reference signal and a measured system output, and then generates an output based on the difference between these signals. A weighted difference signal is computed for each of the proportional, integral, and derivative actions with respect to a set point value that is specified by the user.

Figure 4.8 is an expression of the 2 DoF PID control system. r is a set point variable, e is the error, u is the manipulated variable, d is disturbance, and y is the controlled variable.

F(s) and C(s) are the set point filter and the conventional PID element respectively, and are expressed as follows:

$$F(s) = \frac{1 + (1 - \alpha)T_i\, s + (1 - \beta)T_i\, T_d\, s\, D(s)}{1 + T_i\, s + T_i\, T_d\, s\, D(s)} \tag{4.14}$$

$$C(s) = K_p\left(1 + \frac{1}{T_i s} + T_d\, D(s)\right) \tag{4.15}$$

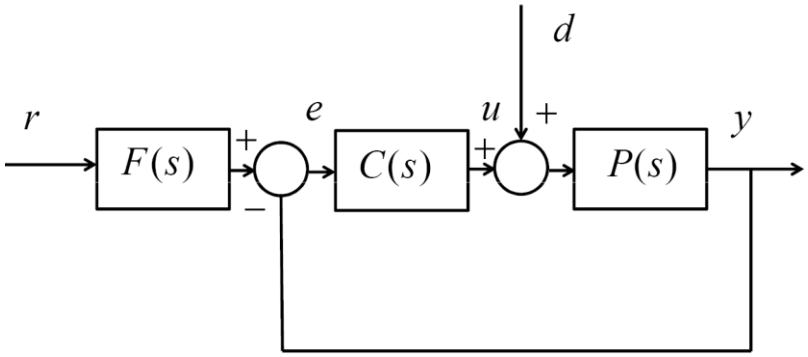

Figure 4.8 - Set point filter type expression of the 2 DoF PID control system

Where,

$$T_d = \frac{K_d}{K_i} \tag{4.16}$$

$$T_i = \frac{K_i}{K_p} \tag{4.17}$$

$$D(s) = \frac{s}{1 + \tau s} \tag{4.18}$$

The set point α is the proportional set point weight. Reducing the value of α will slowly phase out the proportional action on the reference signal.

The set point β, on the other hand, is the derivative set point weight. Reducing the value of this set point will yield a controller with a derivative action on the measured response but not the reference input.

The filter co-efficient determines the pole location of the filter in the derivative action. The proportional, integral, and derivative paths will be explained in section 4.7.

All the parameters mentioned previously are automatically set when tuning the controller. Afterwards, fine adjustments are done manually to achieve optimum control. Table 4.3 shows the parameters of the controller after tuning.

Table 4.3 - Two DoF controller parameters

Proportional Gain	-1.15
Integral Gain	-50007.05
Derivative Gain	1.114e-7
Filter Co-efficient (N)	10395564.21
Set point (b)	1
Set point (c)	1

Figure 4.9 shows the output of the model obtained from system identification after introducing the 2DoF PID controller. The responses are in distinguishable. The overall system block, containing the 2DoF PID controller and the state space system from system identification, has outstanding accuracy when converting values of the current to displacement. These results aid in tracking our system and applying necessary measures to control it actively, as will be shown later in section 3.7.

Both Figures 4.10 and 4.11 emphasize on the accuracy of the final "tracking" system.

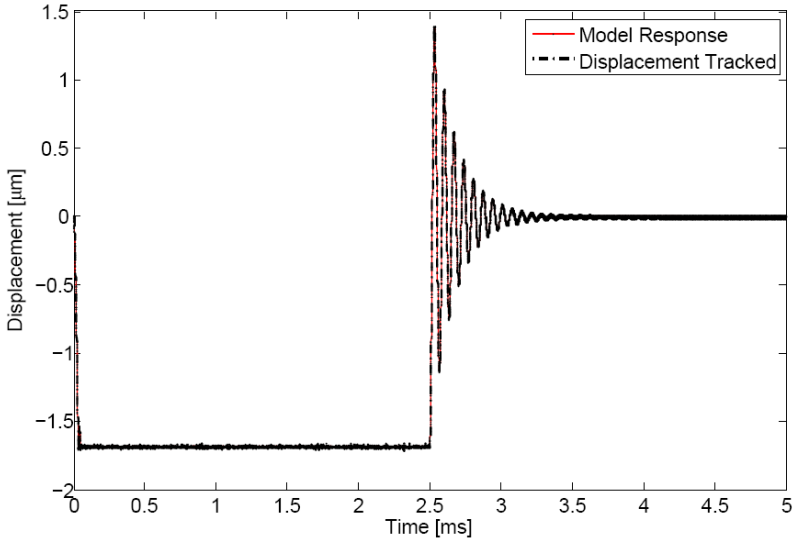

Figure 4.9 - Switch response obtained from system identification vs real system response

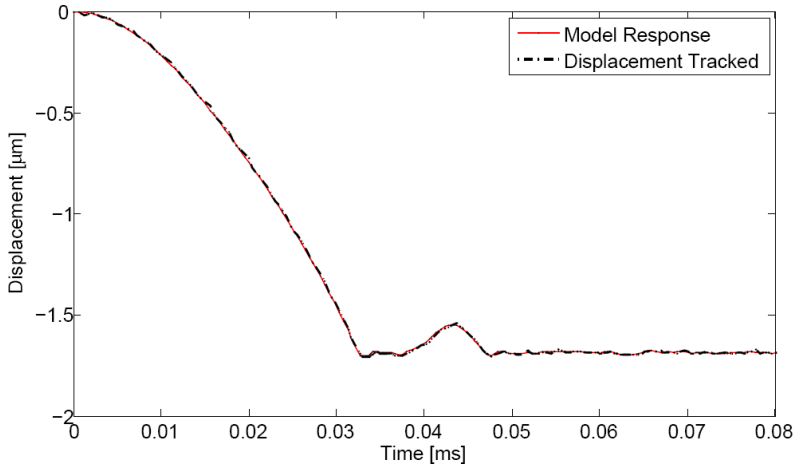

Figure 4.10 - Transient response obtained from system identification

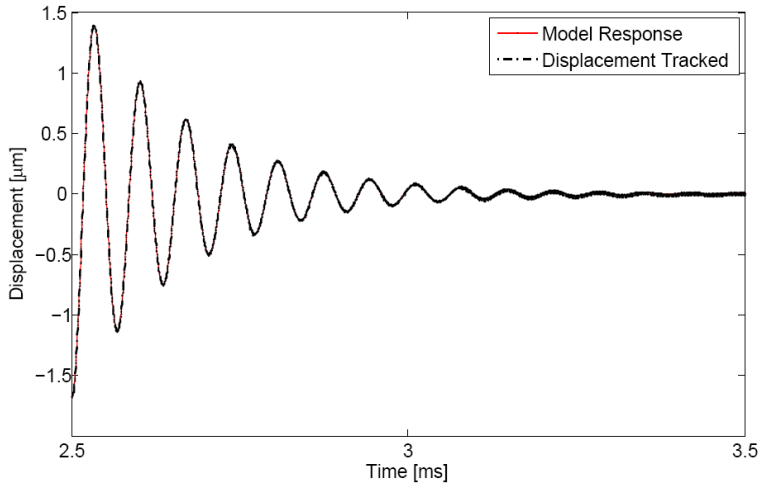

Figure 4.11 - Release response obtained from system identification

4.7 Control

MEMS devices are used in plenty of controllers to control macro systems. Nevertheless, MEMS devices, themselves, are very difficult to control since they combine the structure, actuators, electronics, sensors, and optics on a single substrate. Therefore, adding a sensor and an actuator, to sense and control the operation of a MEMS device, is a complex design decision, not mentioning that a sensor with sampling time enough to capture the MEMS switch dynamics is difficult to manufacture. In addition, at the micro level, the forces acting on the systems are unlike those at the macro level. For instance, the gravity force, which has a significant impact at the macro level, plays a negligible role at the micro level. On the other hand, the governing forces are the surface tension, electrostatic, sticking, and Van Der Waals.

There are mainly two general ways of how systems are controlled, the first is in an open loop manner and the second in a closed loop manner. In open loop, the time and variables are not adjusted based on any feedback from the system. For instance, a car can be controlled to move from point A to point B by calculating the car's velocity, and distance from A to B, then allowing the car to move for a specific amount of time in order to stop at point B. This way of controlling is used in some applications, mainly those with responses that do not change much over time. Nevertheless, open loop control is not reliable enough, since if the variables changed or the time, i.e. the velocity of the car or how long it has been moving, the controller would not react upon these changes since no feedback is sensed, and the system would most probably go unstable. On the other hand, a closed loop system sends a feedback of the systems current position, to a controller that compares this value to a reference value, and manipulates the input of the system in order to minimize the error. This type of controlling the system is much more reliable than the open loop, and it is the type used in this work.

After the modeling is done with a very high accuracy, along with the tracking system, the next step would be to actively control the switch. This process will be executed using the output results from the tracking system, acting as a sensor, according to the following steps:

1. Measure the current of the switch "extracted from the model".
2. Using the current as an input to the system consisting of the state space model, from the system identification, as well as the 2 DoF PID controller model.
3. Feeding the output to the tuned PID controller.
4. Converting the values of displacement into voltage by using a conversion factor, i.e a constant gain.
5. Finally, the obtained voltage values will be fed negatively to the input voltage in order to manipulate the system response as desired.

4.7.1 PID controller design

A PID controller is used considering that its major advantage lies in its simplicity, in addition, the PID is widely used and applied to different types of applications. A PID controller is shown in Figure 4.12, and it consists of 3 main parts:

1. Proportional.
2. Derivative.
3. Integral.

The proportional part is a constant multiplied by the error signal. The effect of the proportional part is reducing the rise time of the system, and the steady state error, however it will not eliminate it.

The integral part will sum the error up and multiply it by a constant. This is used to remove the constant errors in the system. Since no matter how small the errors are, the summation will be significant enough to adjust the controller output. The effect of the integral part will eliminate the steady state error, but it will make the transient response worse. Especially in the case of this study, since the system is very sensitive, the low-magnitude impacts of the switch’s capacitor plates is perceived as error by the integral part of the controller, making the sum a huge value on which if the controller tried to adjust the output, it will destabilize the system. In this case, the integral part is removed and the controller is built upon proportional and derivative parts only.

The derivative part is the rate of change of the error that contributes to the output signal. The derivative part predicts how the error will be based on the previous error, and tries to adjust the controller output. The effect of the derivative part is

increasing the transient response of the system, reducing the overshoot, as well as the stability of the system.

Figure 4.12 along with the equations derived of the closed loop system will clarify the effect of each of the PID controller paths on the process.

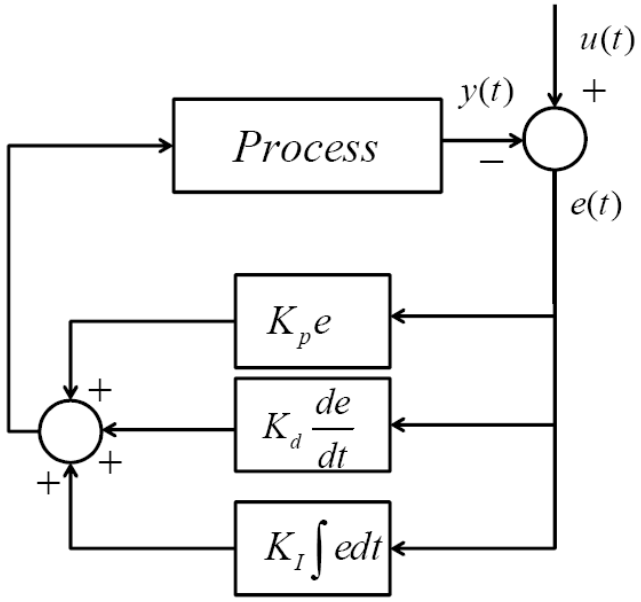

Figure 4.12 -Expression of PID control system.

Below is the general equation governing the mechanical behavior of a system:

$$M\,\ddot{x} + B\,\dot{x} + K\,x = \sum F_{total} \tag{4.19}$$

Taking the transfer function of the previous equation we get:

$$S^2 + \frac{B}{M}\,S + \frac{K}{M} = \sum \frac{F(s)_{total}}{X(s)} \tag{4.20}$$

Where,

$$\frac{B}{M} = 2\,\zeta\,\omega_n \tag{4.21}$$

$$\frac{K}{M} = \omega_n^2 \tag{4.22}$$

ζ is the damping co-efficient of the system, and ω_n is the natural frequency. Finally, the closed loop transfer function of the system is equal to:

$$G_{CL} = \frac{H}{1 + CH} \tag{4.23}$$

Where H is the transfer function of the system, i.e. the reciprocal of the L.H.S of Eq. 4.20, and C is the transfer function of the PID controller, identical to Eq. 4.15. The final simplified form of the closed loop equation is expressed as follows:

$$G_{CL} = \frac{S}{S^3 + (K_d + 2\zeta\omega_n)S^2 + (K_p + \omega_n^2)S + K_i} \tag{4.24}$$

$$(K_d + 2\zeta\omega_n) = (2\zeta\omega_n)_{CL} \tag{4.25}$$

$$(K_p + \omega_n^2) = (\omega_n^2)_{CL} \tag{4.26}$$

As observed, when linking Eqs. 4.21, 4.22, and 4.24, and factoring out the term S , we find that the K_d will alter the overall damping of the system, manipulating the transient response. Whereas, the K_p will alter the stiffness of the system, manipulating the rise time. K_i will be divided by S making it unstable if the system is very sensitive, that is why the integral path is eliminated from the PID in our approach, converting the controller into a PD instead.

Chapter 5 : Results

5.1 Modeling Results

Using dimensions listed in Table 3.1 and the model developed in the foregoing modeling approach, calculated values for variables needed to construct the model given in Equations 3.1 and 3.2 are listed in Table 3.2. Forces acting on the FE model are;

$$w(t) = [\, F_e \; F_{es} \; F_{sd} \,]^T \tag{5.1}$$

Forces in Equation 5.1 are lumped forces applied at the corresponding nodes in the FE model. It is clear from Table 3.2 that the first modal frequency $f_{im}|_{i=1}$ is found to have a value of 14.86 kHz which is in 98.5% in agreement with the experimental value reported by [1]. The remaining modes are also in excellent agreement with experiments. Table 5.1 below lists the calculated parameters used in the modeling.

Table 5.1 - Calculated parameters

Permittivity of Air (ε_0)	8.854e-12 F/m
Net area of the membrane (A)	2.92e-8 m^2
Experimental switch voltage	35 Volts
η	1.87e-4 Pa.s
η_{eff}	1.45e-4 Pa.s
a_c	16.16e-6 m
γ	0.5
$H(\gamma)$	0.71
K_{sf}	9 N/m
γ_{sf}	4.73e-3 kg/s
k_{es}	2256 N/m
$f_{im}\|_{i=1}$	14.86 kHz

5.2 Simulation Results

Estimates of the displacement are fed back through a PD controller to achieve the control target of minimizing closing time while reducing membrane landing impact at pull-in voltage, overshoot, settling time, and pull-out or release. The block diagram of the control scheme is shown in Figure 5.1.

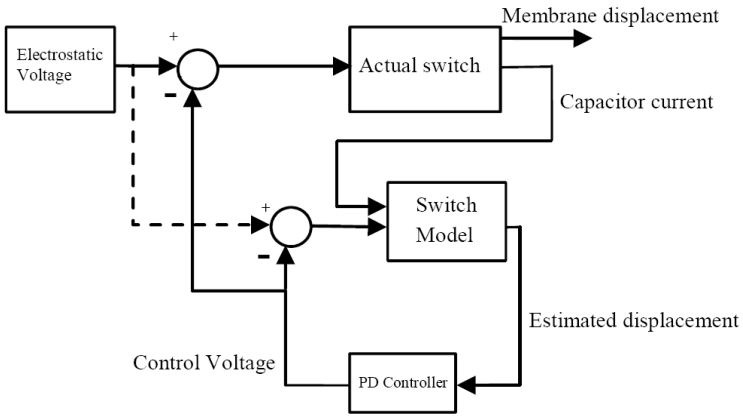

Figure 5.1 -Simulation blocks

Two cases are presented below. In the Figures 5.2, 5.3, and 5.4, we notice that the switch response is relatively slow, this will eliminate the impact as well as the vibrations, however, the closure time is increased significantly. The parameters of the controller used in this case are shown in Table 5.2.

Table 5.2 - Controller parameters case 1

Proportional gain (P)	15000000
Integral gain (I)	0
Derivative gain (D)	-1500
Filter Co-efficient (N)	3444827.3

Figure 5.2 compares the switch's performance before and after the implementation of the controller. As explained in section 4.7.1, introducing the derivative gain will add damping to system response, causing it to become slower and thus avoid impact and early fatigue. On the other hand, the proportional gain reduces the steady-state error significantly.

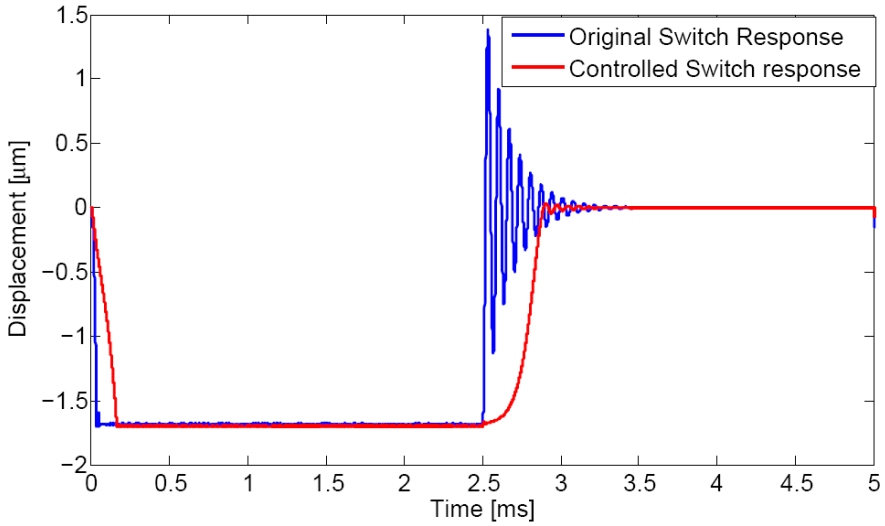

Figure 5.2 -Original vs controlled response case 1

Figure 5.3 emphasizes the pull in response, as noticed, the switch closure time is increased 416%, however the vibrations and impact are avoided.

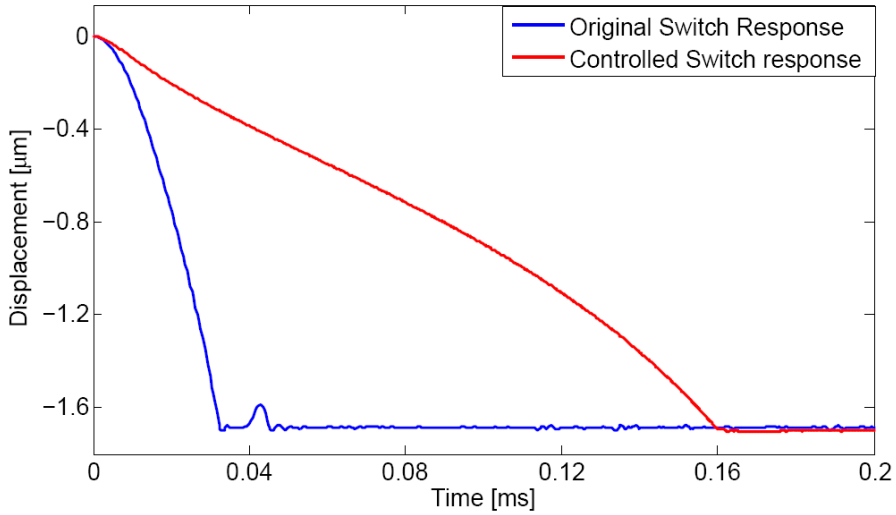

Figure 5.3 -Controlled transient response case 1

Figure 5.4 shows the release response of the switch before and after the implantation of the controller. As noticed, with the controller, the switch vibrates less, the magnitude of these vibrations are reduced by 99% , and the switch returns to its equilibrium point quicker, increasing its life time by avoiding un-necessary fatigue.

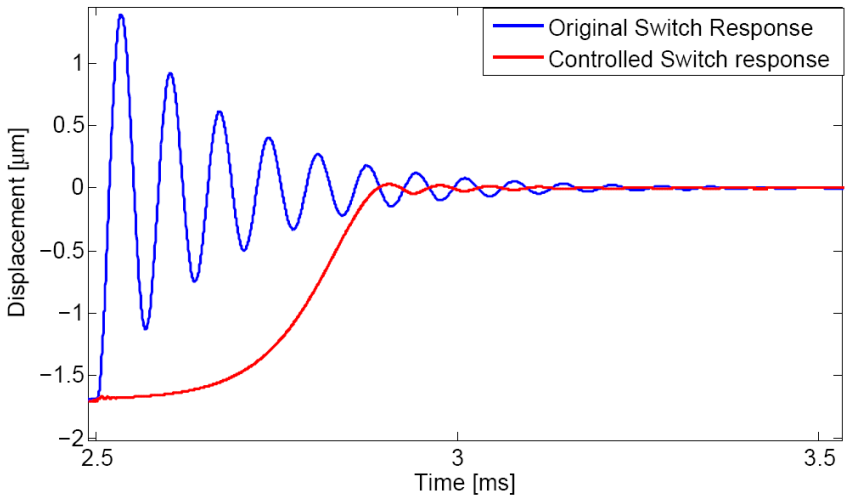

Figure 5.4 -Controlled release response case 1

On the contrary, the second case shows relatively very quick closure time as seen in Figures 5.5, 5.6, and 5.7. However, the vibrations in the release response, although decreased significantly, are not eliminated as shown in Figure 5-4. Depending on the process required, the controller gains can be tuned to achieve optimum response. Table 5.3 shows the controller parameters used in the second case.

Table 5.3 - Controller parameters case 2

Proportional gain (P)	15000000
Integral gain (I)	0
Derivative gain (D)	-300
Filter Co-efficient (N)	3372361.5

As shown in Figures 5.5, 5.6, and 5.7, the switch closure time has increased only 30%, while avoiding impact bouncing. In addition, the vibrations upon release are reduced significantly, an attenuation of 67% is noticed. This is due to decreasing the value of derivative gain five times, while keeping the proportional gain identical.

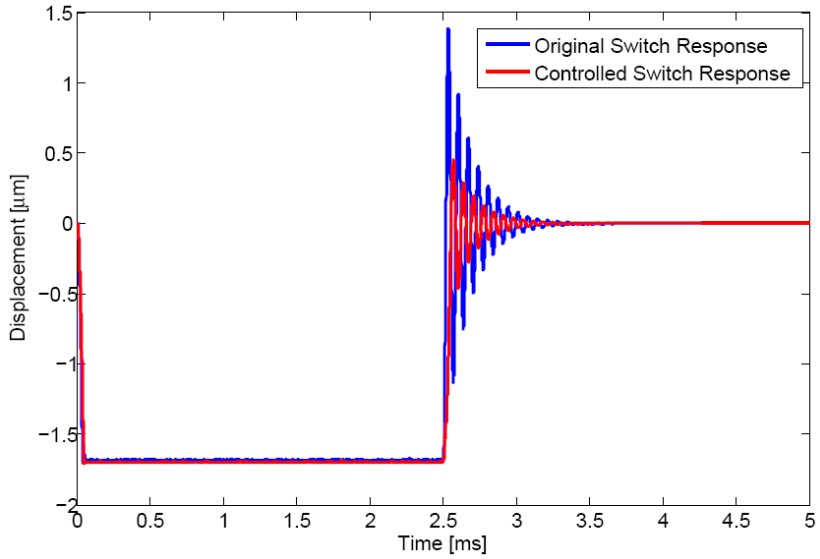

Figure 5.5 -Original vs controlled response case 2

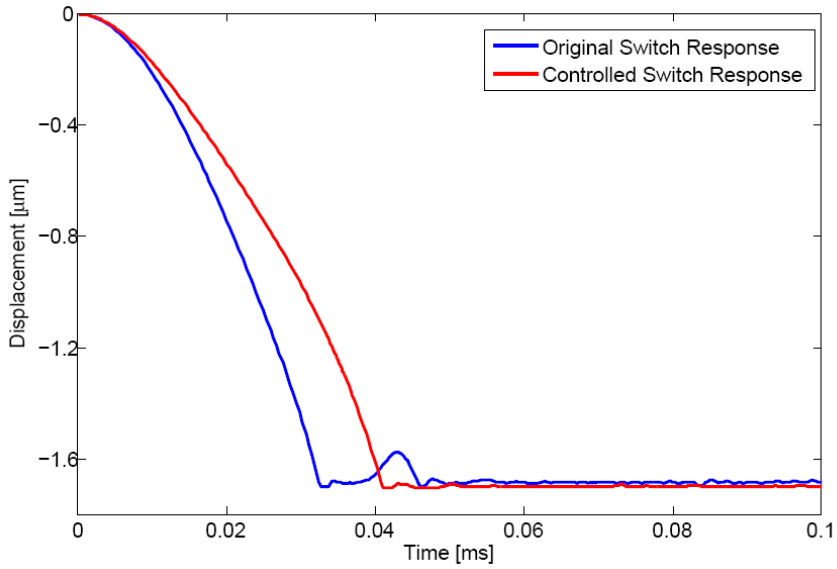

Figure 5.6 -Controlled transient response case 2

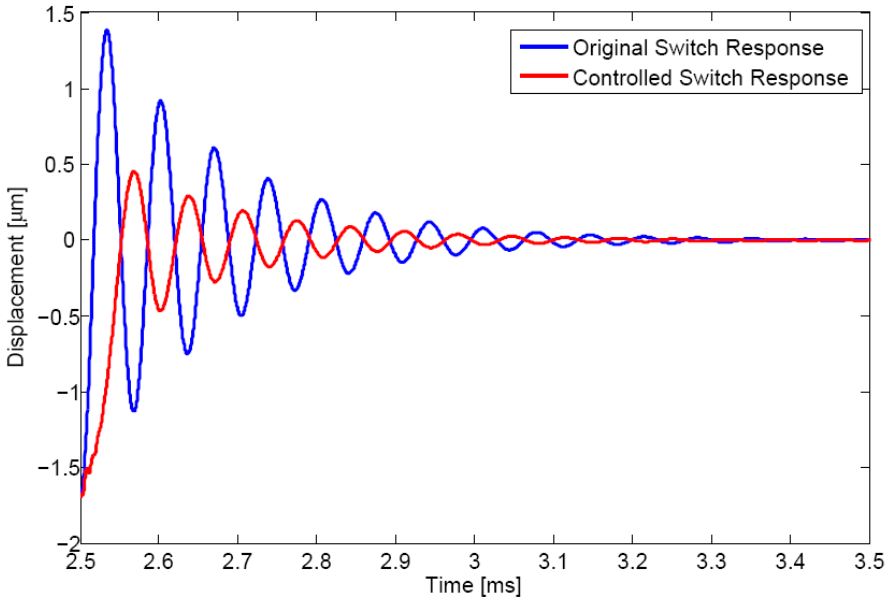

Figure 5.7 -Controlled release response case 2

Chapter 6 : Conclusion

The practical constraints affecting the nature of RF-MEMS switches, such as nonlinearities, size-varying material properties, medium of operation, and external interference, increase the difficulty level associated with modeling RF-MEMS switches, thus, impacting the results' reliability. While there have been plenty of improvements in the field of MEMS modeling, the necessity of having experimental data to compare with still holds, as no details in MEMS modeling are considered minor, and everything needs to be taken into account.

In the SPST RF-MEMS model, the significance of the squeeze film on a non-uniform RF MEMS switch has been introduced after studying two analytical models of an oscillating plate in vacuum and under one atmospheric pressure. Due to membrane's motion, the squeeze film acts as a combination of a spring and a damper, depending on the velocity of the moving membrane and the frequency at which the plate is vibrating. The effect of the squeeze film affects the overshoot and steady state characteristics, as well as displacement phase, which are considered extremely important in designing or controlling the MEM switch. However, the impact response is not consistent with the results shown in [10], and the response is slower when compared to [10], indicating that the Squeeze Film model is not adequate. In [10], it is mentioned that the simulation results are accurate only up to the first bounce of the switch, after that, results are not consistent with experimental data. In order to design a controller for the RF-MEMS switch, a fairly accurate model has to be obtained first. The latter model has to account for all external forces applied on the switch upon actuation. Results have to be in agreement with experimental data before proceeding with controller design. For this reason, and due to the fact that the information on the switch under study is insufficient, the model was discarded, and another model is adopted from [1]. This model has experimental data that contains effects of all external forces needed to examine the validity of the proposed model.

On the other hand, the perforated membrane model introduced using FEA a practical accurate model of an RF-MEMS switch, taking into consideration squeeze film effects and impact forces. Modeling results were comparable with the experimental results with accuracy of 98.6%. Moreover, system identification was performed to create a state space system to convert readings of the current into

displacement referring to the position of the switch's membrane based on Eq. 4.13. The state space model was not accurate enough to be used in tracking the system. This led to the use of a 2DoF PID controller, which adjusted the response of the state space model, improving its reliability.

The proposed tracking system returns accurate information about the position of the capacitor's plate that was used to control the switch's response using a PID controller. Tuning the gains of the PID controller results in different responses of the system. The response can be slowed down to eliminate the impact and vibrations of the switch, this can be used in systems where the closure time of the switch is not very significant. In other applications, where the switch is required to close as fast as possible, the PID gains can be tuned to achieve higher closure time, minimizing the impact and vibrations of the switch, yet not eliminating them.

The fact that the switch response was modified opens endless opportunities in real life applications. However, due to the fact that the system is very sensitive, one should not forget the importance of the system identification's accuracy. In the future, a mean to extract the displacement from the current values might be introduced, giving more accurate information about the membrane's position, and rendering the system identification method inefficient in this case. The modeling technique is valid for different types of RF MEMS switches after some modifications, such as modeling and system identification. This would result in the ability of controlling MEMS switches in more applications, increasing their efficiency and life cycle significantly.

References

[1] M. Niessner, G. Schrag, J. Iannacci, & G. Wachutka, "Macromodel-based simulation and measurement of the dynamic pull-in of viscously damped RF-MEMS switches", Sensors and Actuators A:Physical, vol. 172, pp. 269-279, 2011.

[2] M. Suijlen, J. Van Gils, & M. H. Beijerincka, "Squeeze film damping in the free molecular flow regime with full thermal accommodation," Sensors and Actuators A 156, pp. 171-179, 2009.

[3] A. L. Herrera-May, L. A. Aguilera-Corte, s. L. Garca-Gonzalez, & E. Figueras-Costa, "Mechanical behavior of a novel resonant microstructure for magnetic applications considering the squeeze-film damping," Microsyst Technol, 15:259268, DOI 10.1007/s00542-008-0658-4, 2009.

[4] M. Bao, & H. Yang, "Squeeze film air damping in MEMS," Sensors and Actuators A: Physical, vol. 136, Issue 1, pp. 3-27, ISSN 0924-4247, 10.1016/j.sna.2007.01.008, 2007.

[5] M.Younis, & I. Yagubizade, "The effect of squeeze-film damping on the shock response of clamped-clamped microbeams," Journal of Dynamic Systems, Measurement, and Control, vol. 134, pp. 011-017-1, 7. doi: 10.1115/1.4004789, 2012.

[6] A. Pandey, R. Pratap, & F. Chau, "Analytical solution of the modified Reynolds equation for squeeze film damping in perforated MEMS structures," Sensors and Actuators A: Physical, vol. 135, Issue 2, pp. 839-848, ISSN 0924-4247, 10.1016/j.sna.2006.09.006, 2007.

[7] R. La Rose III, & K. Murphy, "Impact dynamics of MEMS switches," Springer-Verlag; New York, 2009.

[8] A. El-Sinawi, "Active vibration isolation of a flexible structure mounted on a vibrating elastic base.", vol. 271, pp. 323-337, 2003.

[9] A. Nayfeh, & M. Younis, "A new approach to the modeling and simulation of flexible microstructures under the effect of squeeze-film damping," J. Micromech. Microeng., vol. 14, pp. 170-181, 2004.

[10] B. McCarthy, G. Adams, & N. McGruer, "A dynamic model, including contact bounce, of an electrostatically actuated microswitch," J. Microelectromechanical systems. vol. 11, pp. 276-283, 2002.

[11] C. W. Jung, & F. D. Flaviis, "RF-MEMS Capacitive Series Switches of CPW & MSL Configurations for Reconfigurable Antenna Application," Irvine, CA, 2005.

[12] C. W. Jung, & F. D. Flaviis, “Recongurable Scan-Beam Single-Arm Spiral Antenna Integrated with RF-MEMS Switches,” IEEE transactions on antennas and propagation, vol. 54. NO 2, 2006.

[13] S. Fouladi, & R. R. Mansour, “Capacitive RF MEMS switches fabricated in standard 0.35 m CMOS Technolog,” IEEE transactions on microwave theory and techniques, vol. 58, NO. 2, 2010.

[14] H. Seidel, H. Riedel, R. Kolbeck ,G. Muck, W. Kupke, & M. Koniger, “Capacitive silicon accelerometer with highly symmetric design,” Sensors Actuators A 23 3125, 1990.

[15] W. E. Newell, “Miniaturization of tuning forks Science,” 161 13206, 1986.

[16] J. D. Zook, D. W. Burns, H. Guckel, J. J. Sniegowski, R. L. Engelstad, & Z. Feng, “Characteristics of polysilicon resonant microbeams,” Sensors and Actuators, vol. A35, pp. 5159, 1992.

[17] L. X. Zhang, & Y.P. Zhao, “Electromechanical model of RF MEMS switches,” Microsystem Technologies 9, 420426-Springer-Verlag, DOI 10.1007/s00542- 002-0250-2, 2003.

[18] M. Niessner, G. Schrag, G. Wachutka, & J. Iannacci, “Modeling and fast simulation of RF-MEMS switches within standard IC design frameworks,” SISPAD, 17-B.2, 2010.

[19] M. Horowitz, Synthesis of Feedback Systems. Academic Press, 1963.

[20] B. Bovric, F.L. Lewis, W. McCulley, A.Q. Liu, E.S. Kolesar, & D.O. Popa, “Control Issues for Microelectromechanical Systems,” IEEE Control Systems Magazine, 2006.

[21] A. O’Dwyer, “Performance improvement using simple PID controller tuning formulae,” School of Control Systems and Electrical Engineering, Dublin Institute of Technology, Ireland, 2006.

[22] G.P. Liu, & S. Daley, “Optimal-tuning PID control for industrial systems,” Control Engineering Practice, DOI: 10.1016/S0967-0661(01)00064-8, 2001.

[23] K.J. strm, & T. Hgglund, “The future of PID control, Control Engineering Practice,” vol. 9, Issue 11, Pages 1163-1175, ISSN 0967-0661, 2001.

[24] A. Izadbakhsh, S. Rafiei, “Robust Control Methodologies for Optical Micro Electro Mechanical System - New approaches and Comparison,” Power Electronics and Motion Control Conference, 10.1109/EPEPEMC.2008.4635577, 2008.

[25] G. Zhu, J. Penet, & L. Saydy, "Robust Control of an Electrostatically Actuated MEMS in the Presence of Parasitics and Parametric Uncertainties," American Control Conference, 10.1109/EPEPEMC.10.1109/ACC.2006.1656386, 2006.

[26] A. Seleim, E. Abdul Rahman, & G. Heppler, "Dynamics of a Close Loop Controlled MEMS Actuator," Microsystems and Nanoelectronics Research Conference, MNRC 2009. 2nd, 2009.

[27] B. Borovic, C. Hong, A.Q. Liu, L. Xie, & F.L. Lewis, "Control of a MEMS Optical Switch," 43rd IEEE Conference on Decision and Control, 0 7803- 8682-5/04/2004 IEEE, 2004.

[28] W. Gawronski, "Dynamics and Control of Structures," 1st ed. Springer-Verlag; New York, 1998.

[29] L.A. Rocha, L. Mol, E. Cretu, & R.F. Wolffenbuttel, "Experimental Verification of Squeezed-Film Damping Models For MEMS," Dept. Microelectronics, Fac. EEMCS, Delft University of Technology, Mekelweg 4, 2628 CD Delft, The Netherlands, 2009.

[30] S. Halder, C. Palego, Z. Peng, J. Hwang, D. Forehand, & C.Goldsmith, "Compact rf model for transient characteristics of mems capacitive switches," IEEE Transactions on microwave theory and techniques, 57(1), 2009.

[31] V. Kaajakari. Practical MEMS. (1st ed.). Las Vegas, Nevada: small gear publishing, 2009.

[32] R.G. Budynas. Shigleys Mechanical Engineering Design. (8th ed.). USA: Mc-GrawHill Primis publishing. ISBN: 0390764876, 2006.

[33] T. Irvine. "Effective modal mass and participation factors," Vibration data, 2012.

[34] L. Ljung, System Identification Theory for the User Second Edition, PRENTICE HALLL PTR, Upper Saddle River, NJ 07458, 1990.

[35] JL. M. Horowitz, Sunthesis of Feedback Systems Academic Press, 1963.

[36] M. Araki, H. Taguchi.Two-Degree-of-Freedom PID Controllers International Journal of Control, Automation, and Systems Vol. 1, No. 4, 2003.

[37] J. Young. Squeeze-film damping for MEMS structures. MIT Thesis, 1998.

[38] A.H. El-Sinawi, "Vibration attenuation of a flexible beam mounted on a rotating compliant hub," Journal of Systems and Control Engineering, Part I, vol. 218, pp. 121-135, 2004.

Vita

Omar A.H. Awad was born on January 6th, 1990, in Abu Dhabi, United Arab Emirates. He received his high school diploma from Al-Manara Private School in Abudhabi in 2007. He graduated from the American University of Sharjah in 2011 with a B.S degree in Mechanical Engineering. Afterwards, Omar joined the graduate program at the department of Mechanical Engineering at AUS as a GTA (Graduate Teaching Assistant) with a full scholarship. During his study time, he participated in the ICMSSM and submitted 3 conference papers and 2 journal papers about his research findings.